Photocatalytic Performance Evaluation of Bismuth Doped Tin-Dioxide under UV and Direct Sunlight Irradiation for Congo Red Dye Degradation

[1]Nauman Ali*, [1]Adnan khan, [1]Aaisha Riaz, [2,3]Abdullah M. Asiri and [2,3]Tahseen Kamal
[1]*Instituite of chemical science, University of Peshawar, Peshawar, Khyber Pakhthunkhwa, Pakistan.*
[2]*Department of chemistry, Faculty of science, King Abdulaziz University, Jeddah, Saudi Arabia.*
[3]*Center of Excellence for Advanced Materials Research, King Abdulaziz University, Jeddah, Saudi Arabia.*
nali75pk@uop.edu.pk*

(Received on 24th June 2019, accepted in revised form 8th June 2020)

Summary: In the current research work, bismuth doped tin-dioxide (Bi-SnO_2) was prepared by wet chemical co-precipitation method. The synthesized material was used as a photocatalyst in the degradation of congo red dye (CR) in its aqueous solution. The prepared catalyst was used in the uncalcined- and calcined forms for the photocatalytic reaction. The synthesized catalyst in both forms was characterized by UV-visible spectroscopy, scanning electron microscopy (SEM) and X-ray diffraction (XRD). The XRD revealed that the calcination of the Bi-SnO_2 improved its crystallinity. The SEM showed that the Bi-SnO_2 had average size less than 150nm. Photocatalytic degradation of CR dye was carried out under ultra-violet light as well as under sunlight. While testing the photocatalytic degradation performance, it was found that more than 80% of the CR was degraded by using Bi-SnO_2 nanoparticles under both lighting conditions. Moreover, the calcined Bi-SnO_2 nanoparticles showed better photocatalytic performance as compared to its uncalcined form. The present work provides a viable way to make efficient photocatalyst based-on Bi-SnO_2 to employ under UV and sunlight for the degradation of the CR dye without the need of oxidizing or reducing agents.

Key Words: Bismuth doped tin-dioxide, Photocatalytic degradation, UV and sunlight, Hydroxyl free radicals, calcination.

Introduction

Dyes are used to color various products at many industries such as, leather tanning, paper, oils, and textiles [1]. During its processing, dyeing material is released from these industries as a wastewater [2, 3]. Many of these dyes are toxic, thus they create a major environmental problem by contaminating water bodies which adversely affect the living organisms [1-5]. Many types of dyes like acidic, basic, solvent, disperse; vat, sulfur and reactive dyes are used by these industries. Each type of dye has a very peculiar chemistry, structure and specific way of bonding to other materials. According to one of the previous report, as high as 5000 tons of coloring material are annually discharged to the environment by various industries [4]. The manipulation of synthetic dyes in our daily life have increased dramatically as compared to former times [5–7]. These poisonous dyes in the wastewater impart many mutagenic as well as noxious effects on human health [8, 9]. So far, numerous convenient methods have been established for the removal of these dyes from wastewater. For instance, the removal of dyes from wastewater had been performed by adsorption process [10, 11], advanced oxidation processes by using high energy radiations [12], and oxidation methods which involve cavitation and ozonation. Moreover, some other methods like sonophotocatalysis [13], chemical reduction process [14–22], and degradation by biological species including algae, fungi, bacteria also played effective role in the removal of dyes from wastewater [15, 23–28]. Even though, all the above processes mentioned are considered as efficient methods for the dye removal but one of the most effective procedure used for the present work is metal oxide based photocatalytic degradation of the dyes. The transition metal oxides act as a catalyst for the generation of electron which degrades the dyes in the irradiations of the UV or sunlight. These catalyst enhances partial oxidation and degradation of azo dyes [29].

It has been a well-established fact that recent years have seen enormous progress in the field of nanotechnology by introducing various functional materials [30–35]. In the past studies, variety of different metal oxides were synthesized and their ability was tested to photo-degrade different toxic dyes or by using a strong reducing agent [5, 14–16, 29, 36–52]. Among many available semiconductor photocatalysts, tin oxide (SnO_2) is considered as one of the most effective material for advanced environmental applications. In the past, the SnO_2 nanoparticles by a hydrothermal method [53]. The SnO_2 nanoparticles was assessed for the photocatalytic degradation of three different toxic

***To whom all correspondence should be addressed.**

dyes namely eosin red, methylene blue, and congo red (CR) under UV light radiations [53]. The CR was removed from aqueous solution by adsorption on SnO_2 as well as photodegradation. It was reported that the CR was photodegraded by SnO_2 with an efficiency of more than 90% in short time. Similarly, the n-type SnO_2 nanoparticles photo-catalytically degraded the methylene blue and eosin red dyes with high catalytic efficiency [53]. In another report, plasma electrolytic oxidation approach was utilized for the synthesis of TiO_2/SnO_2 photocatalyst which degraded methyl orange dye [54]. According to their results, the TiO_2/SnO_2 nanoparticles were able to photodegrade the methyl orange dye up to 60% in short time. Recently, researchers synthesized the CdS/SnO_2 hybrid photocatalyst nanostructures. They adopted a two-step procedure of co-precipitation followed by hydrothermal treatment for the preparation of hybrid catalyst [55]. The photodegradation efficiency of 95% was achieved for the methyl orange by utilizing it in a small quantity of 0.3g and 50ppm of the methyl orange during their experiments [55]. Similarly, Lee et al (2019) synthesized the Zn_2SnO_4/SnO_2 in the form of urchin-like hollow spheres [56]. They used the hydrothermal process for the preparation of this material and the as synthesized material was annealed at 800˚C to get the crystalline material. Upon using Zn_2SnO_4/SnO_2 photocatalyst, the methylene blue dye was degraded. It was found that the urchin-like Zn_2SnO_4/SnO_2 hollow spheres photodegraded it with more than 80%. Bismuth containing compounds along-with SnO_2 nanostructures have been proved to be versatile catalysts. For example, nanofibers of $SnO_2/Bi_2O_3/BiOI$ were prepared by electrospinning followed by chemical etching technique [57]. The process was performed at room temperature and the synthesized $SnO_2/Bi_2O_3/BiOI$ nanofibers were able to swiftly photodegrade the methyl orange and reduce the Cr (VI) with visible light radiations. All the above stated studies are pointing towards the better photocatalytic properties of the SnO_2 when combined with other photocatalysts or simply doping of the other metals to the SnO_2 crystals [29].

In continuation of the above listed photocatalytic studies, it was attempted to determine the feasibility of the total degradation by a combination of photocatalyst and UV treatment of an azo dye of CR. In the present study, we prepared bismuth doped tin oxide (Bi-SnO_2) nanomaterial for photo-catalysis by co-precipitation followed by annealing method. The prepared material was subjected to different instrumental techniques for characterization and successful preparation of the aimed nanomaterial was confirmed. The photocatalytic degradation of CR in water was assessed by utilizing the calcined and uncalcined Bi-SnO_2 samples.

Experimental

Instruments and Equipments

pH-meter (Model 3505, voltage 9 VAC, Frequency 50/60 Hz, Power 6 VA) was used to determine the pH of the solutions. Magnetic Stirrers (GR BIOTEK MS-HS 250 V AC, Guohua electric appliance Co. LTD) was used to accelerate the mixing process. Digital Balance (Adventurer Ohaus Corp, Pine Brook, NJ USA Power 8-14.5V – 50/60 Hz 6 VA or 9.5-20 V (6 watt)) was used to measure the quantities of the dye during solutions preparation and weigh the photocatalyst doses. UV-Visible Spectrophotometer (company BMS, Model NO 1202 UV-spectrophotometer, Power source AC 110 volt/ 3.15A) was used during the photocatalytic degradation reaction to measure the dye concentration.

Materials

Congo red dye (3,3′-([1,1′-biphenyl]-4,4′-diyl)bis(4-aminonaphthalene-1-sulfonic acid), $C_{32}H_{22}N_6Na_2O_6S_2$, 696.665 g/mol), ethanol, bismuth nitrat penta hydrate ($Bi(NO_3).5H_2O$, 485.07), tin chloride ($SnCl_2.2H_2O$, 225.63g/mol) and ammonium hydroxide (NH_4OH, 35.04g/mol) were bought from Sigma Alrdrich. All the chemicals used in this experimental work were of analytical grade which were used without further purifications. Deionized water was used in the whole experimental work.

Synthesis of bismuth-doped tin oxide nano photocatalysts

The bismuth-doped tin oxide (Bi-SnO_2) photocatalytic nanoparticles were prepared by wet chemical co-precipitation approach. Briefly, $Bi(NO_3).5H_2O$ and $SnCl_2.2H_2O$ salts were used as the bismuth and tin sources, respectively. Appropriate amounts of the $Bi(NO_3).5H_2O$ and $SnCl_2.2H_2O$ salts in a 0.5:9.5 molar ratio were dissolved in deionized water at high speed magnetic stirring. To improve their solubility, hydrochloric acid was added. After complete dissolution, the solution was filtered. Under the magnetic stirring of the solution, the addition of NH_4OH (0.6 M) was done until the solution pH reached 12. As a result, precipitate was formed, then it was cooled and washed several times with deionized water and dried at 80°C. The obtained

product of Bi_x-$Sn_{(1-x)}O_2$ (with x = 0.5) was grinded to fine powder. The obtained fine powder was divided into two equal parts. The calcination process was performed at 600 °C for 4 h at the rate of 5 ºC per min for one part while the other part (as uncalcined form) was used in the further experiments.

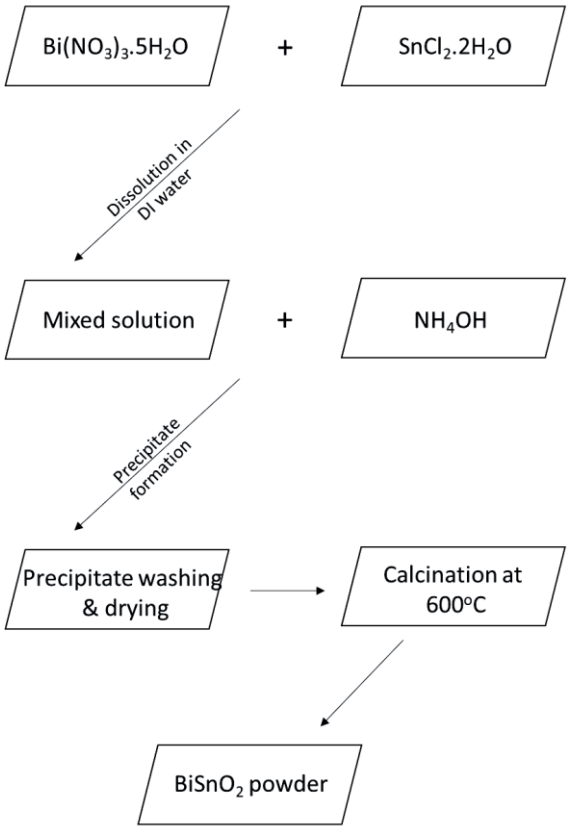

Fig. 1: Preparation steps for the synthesis of Bi-SnO_2.

Characterization of the photocatalysts

Different techniques were used for the characterization of prepared photocatalyts. Scanning electron microscopy (SEM) was used for the morphology determination of the nanomaterial. The samples characterized for morphology on XL 30Philip field emission scanning electron microscope. The crystal structure was confirmed with the help of (PAN-alytical 3040/60 X' Pert Pro Diffractometer) X-ray diffractometer (XRD) equipped with graphite monochromatized Cu Kα radiation with wavelength equal to 1.54 Å. Spectrophotometer BMS (UV-1602) was utilized for determining the CR concentration in aqueous solution during the photocatalytic experiments.

Evaluation of photocatalytic activity for Congo Red degradation

Congo red (CR) stock solution was prepared by dissolving its appropriate amount in de-ionized water to give a final concentration of 0.06mM. The container of solution was covered from light using aluminum foil.

The photocatalytic tests were performed on both the calcined and uncalcined samples by degrading CR as pollutant. The degradation process, 0.5g photocatalyst was mixed with 50 mL aqueous solution of CR (0.06mM) and the container was charged with magnetic stirrer to constantly disperse the photocatalyst in the reaction medium. An initial reading of this CR solution was recorded by UV-visible spectrophotometer. The mixture was then exposed to a 250 W Xe lamp for 3 h. At constant interval of time, 3mL of the solution was withdrawn from the reaction medium which was analyzed by UV-visible spectrophotometer. The degradation of the CR was estimated by the following equation,

$$\text{Degradation (\%)} = \frac{C_0 - C_t}{C_0} \times 100 = \frac{A_0 - A_t}{A_0} \times 100 \quad \text{(Equation 1)}$$

where C_0 and C_t represent the concentration of CR solution at time zero and time t which are proportional to the Absorbance values at λmax 497 nm (A_0 and A_t represent the absorbance values at time zero and time t.)

Similar procedure was used for another reaction where sunlight was used instead of simulated light from 250 W Xe lamp. Sunlight experiments were performed during day-time between 10:00 AM to 2:00PM in the institute lawn where the beaker contents were exposed to the clear sky sunlight. It is important to note that prior to the photocatalytic reaction, the CR + Bi-SnO_2 mixture was placed in dark under stirring for about 30 min to attain maximum adsorption-desorption equilibrium.

Results and Discussion

Characterization of the photocatalytic Bi-SnO_2 nanoparticles

The calcined and un-calcined product was characterized by various techniques as detailed in the proceeding text.

Structural characterization by X-ray Diffraction analysis

Identification and phase composition of calcined Bi-SnO_2 were investigated by XRD method. Fig. 2a and b show the XRD patterns of the uncalcined and calcined Bi-SnO_2 powders, respectively. The XRD pattern of unclaimed Bi-SnO_3 represents irregular crystal size or typical peaks for polycrystalline material. Usually, on XRD patterns of as synthesized metal oxide, it is difficult to observe the diffractions because of the extremely small particle size in the sample. This observation is in line of previously reported data on the synthesis of the transition metal or their oxide nanoparticles [41, 58]. The peaks appeared after annealing the sample at T > 300-600°C in XRD patterns typical for polycrystalline material. It was observed that diffraction peaks appeared after drying the Bi-SnO_2 samples at 80°C. However, after calcination, the as synthesized and dried sample at temperature of 600°C, the XRD pattern showed clear diffractions. The peaks observed at 2θ positions of 26.55, 33.82, 37.84, 51.87, 54.62, 61.79, 65.59, 71.32 and 78.82 which represent to (110), (101), (200), (211), (220), (301), (320) and (321) reflection planes of the tetragonal rutile phase of SnO_2, respectively (JCPDS card #: 41-1445). No peaks from the impurity such as oxides of bismuth or tin were detected which show that the current method could be used effectively for the synthesis of the Bi-SnO_2 photocatalyst.

SEM Analysis

The SEM study was performed for the morphology and size of the Bi-SnO_2 photocatalytic nanoparticles. Fig 3a and b show the SEM images of the uncalcined and calcined samples of Bi-SnO2 nanoparticles. The uncalcined Bi-SnO_2 nanoparticle are present in larger clusters and in agglomerated form. After calcination of Bi-SnO_2 at 600 °C for 3 hs, the agglomerated form changed to smaller sized nanoparticles. The porosity was a little greater in uncalcined Bi-SnO_2 than calcined photocatalyst. The scanning electron microscopy results of both samples showed that the size of nanoparticle is less than 150nm.

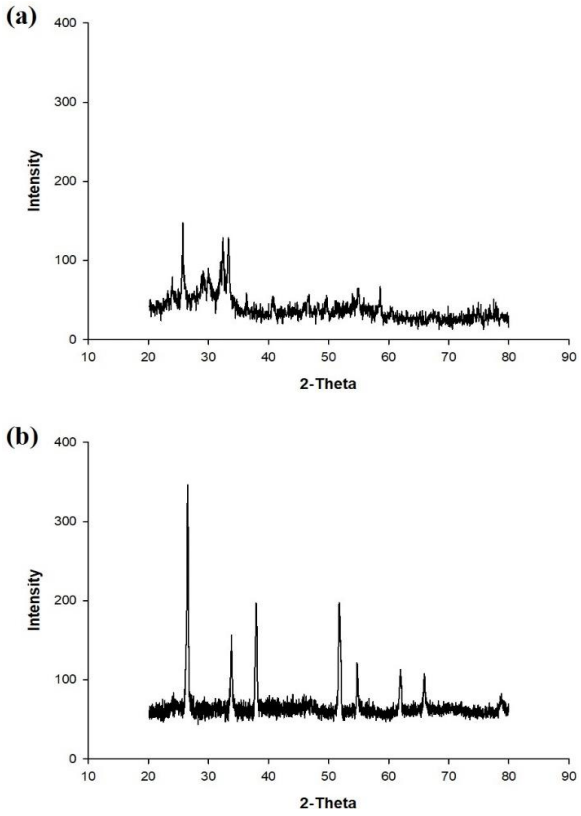

Fig. 2: XRD patterns of (a) uncalcined and (b) calcined Bi-SnO_2.

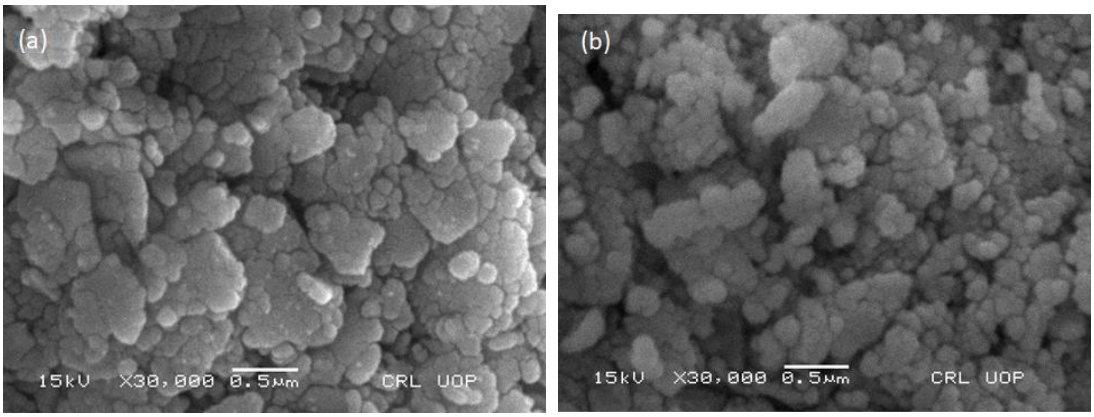

Fig. 3: SEM images of (a) uncalcined and (b) calcined Bi-SnO_2.

Band gap of bismuth-doped tin dioxide

The band gap of photocatalysts was calculated by dispersing (sonicated for two h) 0.02 g of the sample in 20 mL distilled water as well as 2mL of H_2SO_4. The UV-visible spectra was recorded from a fresh suspension. Fig 4a shows absorption spectrum of Bi-SnO_2 nanoparticles suspension. From the graph, a portion of wavelength which gives fundamental peak was selected and *Tauc* plot was drawn having absorbance co-efficient on y-axis and binding energy on x-axis. The band gap was calculated from Tauc's equation given below,

$$\alpha h\nu = A (h\nu - Eg)^n \qquad \text{(Equation 2)}$$

where 'α' is absorption coefficient, 'A' is constant (2 for direct and 1/2 for indirect band gap semiconductors), hν is the photon energy and Eg is band gap energy. A plot between $(\alpha h\nu)^2$ and hν was obtained and the band gap was determined by taking the intercept extrapolation to zero absorption with photon energy axis.

Photodegradation of congo red dye

The CR dye degradation by the photocatalyst was assessed in its aqueous solution as model chemical. Photocatalysis is the best technique for the effective degradation of CR and other dye pollutants. It is based on the photogeneration of positive holes and separated electrons in semiconductor particles. These negatively charged electrons either recombine inside the particle or move to the upper surface and here they react with adsorbed molecules. Positive holes help in oxidizing organic compounds, while electrons mainly cause reducing molecular oxygen to superoxide radical anions. Recombination of photogenerated electrons and positive holes inside the semiconductor particles are accountable for the relatively less quantum yield of photocatalytic reaction. CR is characterized by an azo group which has carcinogenic and toxic effects. This dye is widely used in the laboratories and has been used as model dye in the evaluation of the photocatalysts and other catalysts [40]. Photocatalytic degradation of CR was carried out under both sun-light and UV-light emitting lamp. The effect of photocatalysis under sun-light and UV-lamp has been investigated for different intervals of time by recording the UV-visible spectra from the CR solution. For this purpose, 50mL solution of 0.06mM CR concentration was taken in a vial along with the measured 0.5g amount of photocatalyst. The mixture of CR solution and Bi-SnO_2 nanoparticles was placed on stirring plate with continued stirring process in dark for 30 min. A UV-visible spectrum was recorded before starting this process. Similarly, another UV-visible spectrum was recorded after 30 min and the decrease in the concentration was determined which was due to the adsorption of the CR molecules on the Bi-SnO_2 nanoparticles. After this, the CR solution containing Bi-SnO_2 was brought under the light conditions (either sun-light or UV light). The UV-visible absorption spectra were continuously recorded in the range of 250-700 nm by UV-visible spectrophotometer until the CR solution looked visibly transparent. Fig 5a shows the UV-visible spectra of the CR dye solution which were continuously measured during the photocatalytic reaction by a calcined Bi-SnO_2 nanoparticles in the presence of sunlight. The CR solution showed two absorption peaks at 344 and 497 nm in its UV-visible spectrum. The high intensity peak at 497 nm was considered as λ_{max} and it was used in equation 1. An absorption peak at 497 nm continuously decreased with the reaction time. As reported earlier[59], a photon of proper energy interacts with the molecules of dye in water in the existence of photocatalyst and releases a hydroxyl radical during the exposure to light. By the interaction of these free radicals with the molecules of dye, the dye degrades with time. This advanced photo activated chemical reaction causes the oxidation of dye and resulted in degradation which observed by the bleaching of dye determined by the UV-spectra. The degradation percentage of different photocatalysts in different irradiation sources is compared in the following Figs. Fig 5b shows degradation of Congo red with uncalcined Bi-SnO_2 in UV light. It is clear from this Fig that uncalcined Bi-SnO_2 photo-catalytically degraded the CR dye up to 82% in the sunlight while 75% degradation was achieved in the UV-light. Fig 5c represents degradation of CR red with calcined Bi-SnO_2 in UV- and sun-light. It is apparent from this Fig that calcined Bi-SnO_2 photo-catalytically degraded the CR dye to more than 85% in 140 min during both the lighting conditions. Based on the results obtained, it can be concluded that the annealing treatment for the Bi-SnO_2 nanomaterial effectively improves their photocatalytic properties.

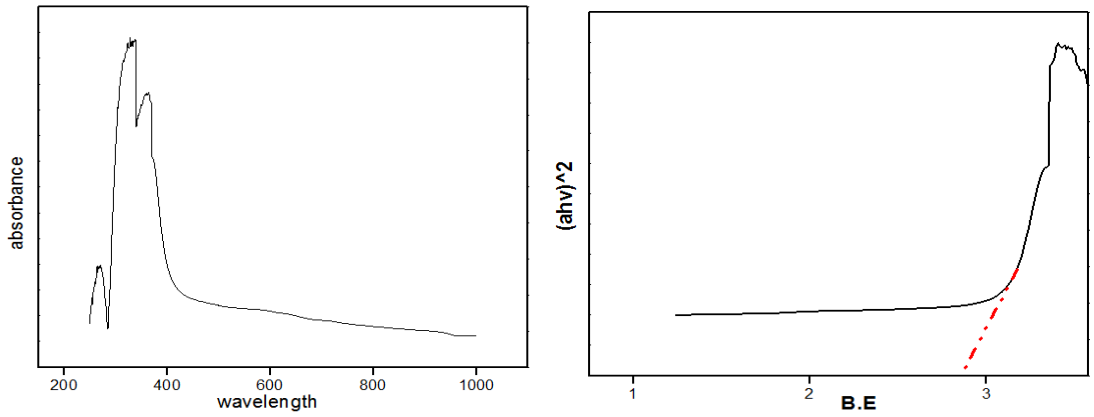

Fig. 4: (a) Uv-visible absorption spectrum of Bi-SnO_2 and (b) corresponding Tauc plot.

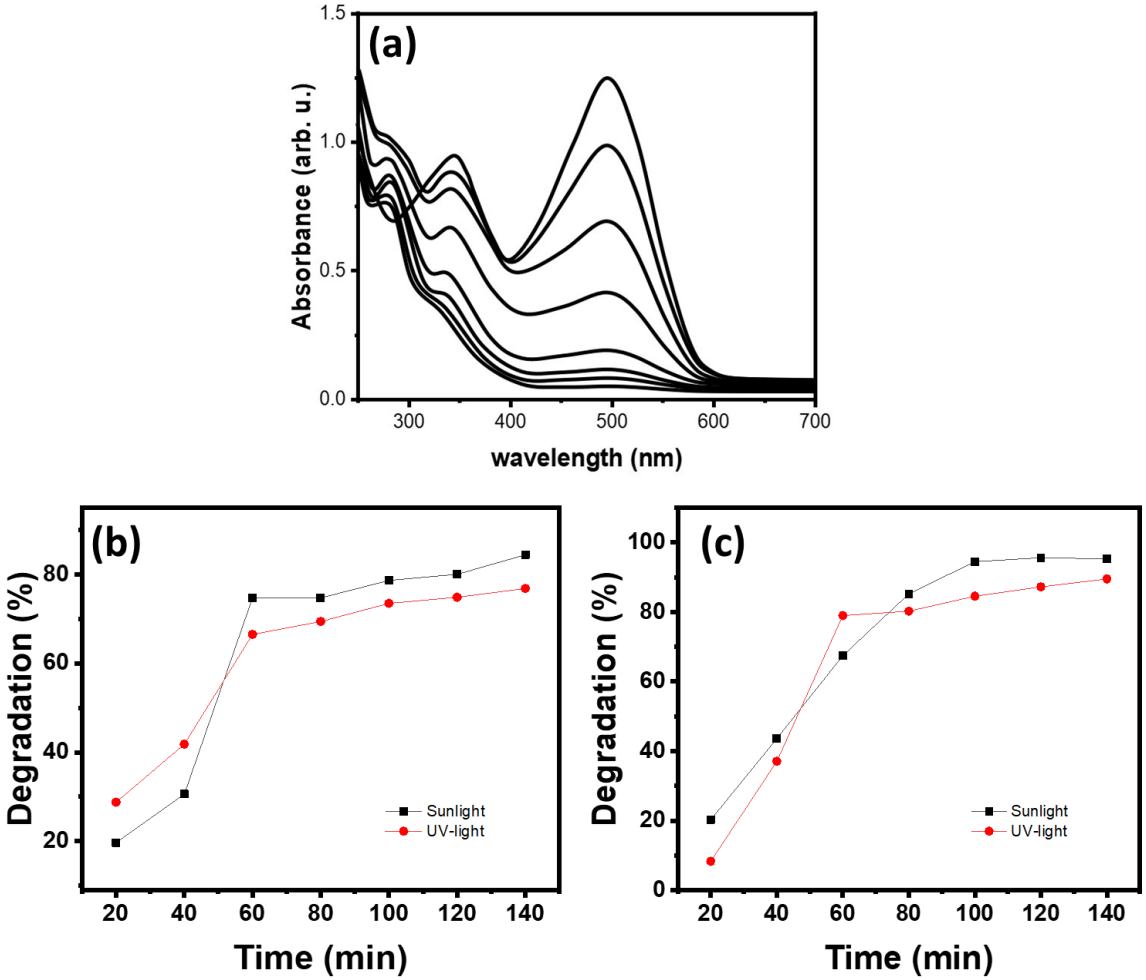

Fig. 5: Typical UV-visible spectra of the CR degradation by a calcined Bi-SnO_2 photocatalyst in the sunlight (a), percent degradation of the CR in the presence of (b) uncalcined and (c) calcined Bi-SnO_2 nanoparticles. The panels (b-c) consist of experimentally determined percent degradation values in both the lighting conditions.

Conclusion

A metal oxide photocatalyst (Bi-SnO_2) was by wet chemical co-precipitation method for the degradation of CR dye. The successful Bi-SnO_2 nanomaterial preparation was confirmed by XRD technique. The degradation of CR dye was carried out under two light sources which were UV-light emitting lamp and direct sunlight. The photodegradation efficiency of the Bi-SnO_2 photocatalyst was investigated and it was found that after 140 min the degradation percentage of the prepared catalyst was 85% and 95% by calcined Bi-SnO_2. The prepared calcined photocatalyst showed superior photocatalytic performance in sunlight. The greatly enhance photodegradation performance to CR are mainly attributed to the enhanced light absorbance of the photocatalyst and plentiful active adsorption sites due to high surface area. Both hydroxyl radicals and photogenerated holes were identified as the main active species in the photo-decolorization process of the CR dye. The greater photocatalytic performance of the specified photocatalyst exhibit great potential on photodegradation of other organic pollutants under sun-light.

References

1. H. Bahria and Y. Erbil, UV technology for use in textile dyeing and printing: Photocured applications, *Dyes Pigments* **134**, 442 (2016).
2. T. Kamal, High performance NiO decorated graphene as a potential H-2 gas sensor, *J. Alloys Compd.* **729**, 1058 (2017).
3. T. Kamal, S. B. Khan, S. Haider, Y. G. Alghamdi, and A. M. Asiri, Thin layer chitosan-coated cellulose filter paper as substrate for immobilization of catalytic cobalt nanoparticles, *Int. J. Biol. Macromol.* **104**, 56 (2017).
4. A. Pirkarami and M. E. Olya, Removal of dye from industrial wastewater with an emphasis on improving economic efficiency and degradation mechanism, *J. Saudi Chem. Soc.* **21**, S179 (2017).
5. T. Kamal, M. Ul-Islam, S. B. Khan, and A. M. Asiri, Adsorption and photocatalyst assisted dye removal and bactericidal performance of ZnO/chitosan coating layer, *Int. J. Biol. Macromol.* **81**, 584 (2015).
6. E. Forgacs, T. Cserháti, and G. Oros, Removal of synthetic dyes from wastewaters: a review, *Environ. Int.* **30**, 953 (2004).
7. T. Kamal, I. Ahmad, S. B. Khan, and A. M. Asiri, Bacterial cellulose as support for biopolymer stabilized catalytic cobalt nanoparticles, *Int. J. Biol. Macromol.* **135,** 1162 (2019).
8. T. Kamal, S.-Y. Park, M.-C. Choi, Y.-W. Chang, W.-T. Chuang, and U.-S. Jeng, An in-situ simultaneous SAXS and WAXS survey of PEBAX (R) nanocomposites reinforced with organoclay and POSS during uniaxial deformation, *Polymer* **53**, 3360 (2012).
9. T. Kamal, Aminophenols formation from nitrophenols using agar biopolymer hydrogel supported CuO nanoparticles catalyst, *Polym. Test.* **77**, 105896 (2019).
10. M. S. Ahmed, T. Kamal, S. A. Khan, Y. Anwar, M. T. Saeed, A. M. Asiri, and S. B. Khan, Assessment of Anti-bacterial Ni-Al/chitosan Composite Spheres for Adsorption Assisted Photo-Degradation of Organic Pollutants, *Curr. Nanosci.* **12,** 569 (2016).
11. S. B. Khan, S. A. Khan, H. M. Marwani, E. M. Bakhsh, Y. Anwar, T. Kamal, A. M. Asiri, and K. Akhtar, Anti-bacterial PES-cellulose composite spheres: dual character toward extraction and catalytic reduction of nitrophenol, *Rsc Adv.* **6**, 110077 (2016).
12. M. A. Rauf and S. S. Ashraf, Radiation induced degradation of dyes—An overview, *J. Hazard. Mater.* **166**, 6 (2009).
13. N. J. Bejarano-Pérez and M. F. Suárez-Herrera, Sonophotocatalytic degradation of congo red and methyl orange in the presence of TiO2 as a catalyst, *Ultrason. Sonochem.* **14**, 589 (2007).
14. T. Kamal, I. Ahmad, S. B. Khan, and A. M. Asiri, Synthesis and catalytic properties of silver nanoparticles supported on porous cellulose acetate sheets and wet-spun fibers, *Carbohydr. Polym.* **157**, 294 (2017).
15. F. Ali, S. B. Khan, T. Kamal, Y. Anwar, K. A. Alamry, and A. M. Asiri, Anti-bacterial chitosan/zinc phthalocyanine fibers supported metallic and bimetallic nanoparticles for the removal of organic pollutants, *Carbohydr. Polym.* **173**, 676 (2017).
16. F. U. Khan, Asimullah, S. B. Khan, T. Kamal, A. M. Asiri, I. U. Khan, and K. Akhtar, Novel combination of zero-valent Cu and Ag nanoparticles @ cellulose acetate nanocomposite for the reduction of 4-nitro phenol, *Int. J. Biol. Macromol.* **102**, 868 (2017).
17. H. W. Ha, A. Choudhury, T. Kamal, D.-H. Kim, and S.-Y. Park, Effect of Chemical Modification of Graphene on Mechanical, Electrical, and Thermal Properties of Polyimide/Graphene Nanocomposites, *Acs Appl. Mater. Interfaces* **4**, 4623 (2012).
18. T. Kamal, I. Ahmad, S. B. Khan, and A. M. Asiri, Agar hydrogel supported metal

nanoparticles catalyst for pollutants degradation in water, *Desalination Water Treat.* **136**, 290 (2018).
19. M. S. J. Khan, T. Kamal, F. Ali, A. M. Asiri, and S. B. Khan, Chitosan-coated polyurethane sponge supported metal nanoparticles for catalytic reduction of organic pollutants, *Int. J. Biol. Macromol.* **132**, 772 (2019).
20. T. Kavitha, S. Kumar, V. Prasad, A. M. Asiri, T. Kamal, and M. Ul-Islam, NiO powder synthesized through nickel metal complex degradation for water treatment, *Desalination Water Treat.* **155**, 216 (2019).
21. M. S. J. Khan, S. B. Khan, T. Kamal, and A. M. Asiri, Agarose biopolymer coating on polyurethane sponge as host for catalytic silver metal nanoparticles, *Polym. Test.* **78**, 105983 (2019).
22. T. Kamal, I. Ahmad, S. B. Khan, and A. M. Asiri, Agar hydrogel supported metal nanoparticles catalyst for pollutants degradation in water, *Desalination Water Treat.* **136**, 290 (2018).
23. C. G. Boer, L. Obici, C. G. M. de Souza, and R. M. Peralta, Decolorization of synthetic dyes by solid state cultures of Lentinula (Lentinus) edodes producing manganese peroxidase as the main ligninolytic enzyme, *Bioresour. Technol.* **94**, 107 (2004).
24. T. Ito, Y. Shimada, and T. Suto, Potential use of bacteria collected from human hands for textile dye decolorization, *Water Resour. Ind.* **20**, 46 (2018).
25. Md. E. Karim, K. Dhar, and Md. T. Hossain, Decolorization of Textile Reactive Dyes by Bacterial Monoculture and Consortium Screened from Textile Dyeing Effluent, *J. Genet. Eng. Biotechnol.* **16**, 375 (2018).
26. M. Ul-Islam, M. W. Ullah, S. Khan, T. Kamal, S. Ul-Islam, N. Shah, and J. K. Park, Recent Advancement in Cellulose based Nanocomposite for Addressing Environmental Challenges, *Recent Pat. Nanotechnol.* **10**, 169 (2016).
27. T. Kamal, N. Ali, A. A. Naseem, S. B. Khan, and A. M. Asiri, Polymer Nanocomposite Membranes for Antifouling Nanofiltration, *Recent Pat. Nanotechnol.* **10**, 189 (2016).
28. S. A. Khan, S. B. Khan, T. Kamal, A. M. Asiri, and K. Akhtar, Recent Development of Chitosan Nanocomposites for Environmental Applications, *Recent Pat. Nanotechnol.* **10**, 181 (2016).
29. T. Kamal, Y. Anwar, S. B. Khan, M. T. S. Chani, and A. M. Asiri, Dye adsorption and bactericidal properties of TiO2/chitosan coating layer, *Carbohydr. Polym.* **148**, 153 (2016).
30. E.-J. Choi, Y.-H. Seo, T. Kamal, S.-Y. Park, and J. Watanabe, Cybotactic nematic phase in main-chain polyesters with bent-core mesogens, *Polymer* **55**, 1931 (2014).
31. M. T. S. Chani, K. S. Karimov, S. B. Khan, T. Kamal, and A. M. Asiri, Synthesis and Pressure Sensing Properties of Pristine Zinc Oxide Nanopowder and its Blend with Carbon Nanotubes, *Curr. Nanosci.* **12**, 586 (2016).
32. S.-Y. Park, T. Kavitha, T. Kamal, W. Khan, T. Shin, and B. Seong, Self-Assembly of dPS-Liquid Crystalline Diblock Copolymer in a Nematic Liquid Crystal Solvent, *Macromolecules* **45**, 6168 (2012).
33. T. Kamal and S.-Y. Park, A liquid crystal polymer based single layer chemo-responsive actuator, *Chem. Commun.* **50**, 2030 (2014).
34. T. Kamal and S. Park, Shape-Responsive Actuator from a Single Layer of a Liquid-Crystal Polymer, *Acs Appl. Mater. Interfaces* **6**, 18048 (2014).
35. M. Omer, T. Kamal, H.-H. Cho, D.-K. Kim, and S.-Y. Park, Preparation and structure of nylon 4/6 random-copolymer nanofibers, *Macromol. Res.* **20**, 810 (2012).
36. I. Ahmad, S. B. Khan, T. Kamal, and A. M. Asiri, Visible light activated degradation of organic pollutants using zinc–iron selenide, *J. Mol. Liq.* **229**, 429 (2017).
37. T. Kamal, S. B. Khan, S. Haider, Y. G. Alghamdi, and A. M. Asiri, Thin layer chitosan-coated cellulose filter paper as substrate for immobilization of catalytic cobalt nanoparticles, *Int. J. Biol. Macromol.* **104**, 56 (2017).
38. T. Kavitha, S. Haider, T. Kamal, and M. Ul-Islam, Thermal decomposition of metal complex precursor as route to the synthesis of Co3O4 nanoparticles: Antibacterial activity and mechanism, *J. Alloys Compd.* **704**, 296 (2017).
39. M. Pervaiz, I. Ahmad, M. Yousaf, S. Kirn, A. Munawar, Z. Saeed, A. Adnan, T. Gulzar, T. Kamal, A. Ahmad, and A. Rashid, Synthesis, spectral and antimicrobial studies of amino acid derivative Schiff base metal (Co, Mn, Cu, and Cd) complexes, *Spectrochim. Acta. A. Mol. Biomol. Spectrosc.* **206**, 642 (2019).
40. T. Kamal, S. B. Khan, and A. M. Asiri, Synthesis of zero-valent Cu nanoparticles in the chitosan coating layer on cellulose microfibers: evaluation of azo dyes catalytic reduction, *Cellulose* **23**, 1911 (2016).
41. T. Kamal, S. B. Khan, and A. M. Asiri, Nickel nanoparticles-chitosan composite coated cellulose filter paper: An efficient and easily recoverable dip-catalyst for pollutants degradation, *Environ. Pollut.* **218**, 625 (2016).

42. S. Haider, T. Kamal, S. B. Khan, M. Omer, A. Haider, F. U. Khan, and A. M. Asiri, Natural polymers supported copper nanoparticles for pollutants degradation, *Appl. Surf. Sci.* **387**, 1154 (2016).
43. S. B. Khan, F. Ali, T. Kamal, Y. Anwar, A. M. Asiri, and J. Seo, CuO embedded chitosan spheres as antibacterial adsorbent for dyes, *Int. J. Biol. Macromol.* **88**, 113 (2016).
44. N. Ali, Awais, T. Kamal, M. Ul-Islam, A. Khan, S. J. Shah, and A. Zada, Chitosan-coated cotton cloth supported copper nanoparticles for toxic dye reduction, *Int. J. Biol. Macromol.* **111**, 832 (2018).
45. F. Ali, S. B. Khan, T. Kamal, Y. Anwar, K. A. Alamry, and A. M. Asiri, Bactericidal and catalytic performance of green nanocomposite based-on chitosan/carbon black fiber supported monometallic and bimetallic nanoparticles, *Chemosphere* **188**, 588 (2017).
46. S. A. Khan, S. B. Khan, T. Kamal, M. Yasir, and A. M. Asiri, Antibacterial nanocomposites based on chitosan/Co-MCM as a selective and efficient adsorbent for organic dyes, *Int. J. Biol. Macromol.* **91**, 744 (2016).
47. I. Ahmad, T. Kamal, S. B. Khan, and A. M. Asiri, An efficient and easily retrievable dip catalyst based on silver nanoparticles/chitosan-coated cellulose filter paper, *Cellulose* **23**, 3577 (2016).
48. A. Haider, S. Haider, I.-K. Kang, A. Kumar, M. R. Kummara, T. Kamal, and S. S. Han, A novel use of cellulose based filter paper containing silver nanoparticles for its potential application as wound dressing agent, *Int. J. Biol. Macromol.* **108**, 455 (2018).
49. F. Ali, S. B. Khan, T. Kamal, K. A. Alamry, E. M. Bakhsh, A. M. Asiri, and T. R. A. Sobahi, Synthesis and characterization of metal nanoparticles templated chitosan-SiO2 catalyst for the reduction of nitrophenols and dyes, *Carbohydr. Polym.* **192**, 217 (2018).
50. F. Ali, S. B. Khan, T. Kamal, K. A. Alamry, and A. M. Asiri, Chitosan-titanium oxide fibers supported zero-valent nanoparticles: Highly efficient and easily retrievable catalyst for the removal of organic pollutants, *Sci. Rep.* **8**, 6260 (2018).
51. F. Ali, S. B. Khan, T. Kamal, K. A. Alamry, A. M. Asiri, and T. R. A. Sobahi, Chitosan coated cotton cloth supported zero-valent nanoparticles: Simple but economically viable, efficient and easily retrievable catalysts, *Sci. Rep.* **7**, 16957 (2017).
52. F. Ali, S. B. Khan, T. Kamal, Y. Anwar, K. A. Alamry, and A. M. Asiri, Bactericidal and catalytic performance of green nanocomposite based on chitosan/carbon black fiber supported monometallic and bimetallic nanoparticles, *Chemosphere* **188**, 588 (2017).
53. D. Zhao and X. Wu, Nanoparticles assembled SnO2 nanosheet photocatalysts for wastewater purification, *Mater. Lett.* **210**, 354 (2018).
54. S. Stojadinović, N. Tadić, N. Radić, B. Grbić, and R. Vasilić, TiO2/SnO2 photocatalyst formed by plasma electrolytic oxidation, *Mater. Lett.* **196**, 292 (2017).
55. Ch. Venkata Reddy, R. V. S. S. N. Ravikumar, G. Srinivas, J. Shim, and M. Cho, Structural, optical, and improved photocatalytic properties of CdS/SnO2 hybrid photocatalyst nanostructure, *Mater. Sci. Eng. B* **221**, 63 (2017).
56. J. W. Lee, S.-H. Nam, J.-H. Yu, D. I. Kim, R. H. Jeong, and J.-H. Boo, Morphological modulation of urchin-like Zn2SnO4/SnO2 hollow spheres and their applications as photocatalysts and quartz crystal microbalance measurements, *Appl. Surf. Sci.* **474**, 78 (2019).
57. K. Wang, Z. Qian, and W. Guo, Multi-heterojunction of SnO2/Bi2O3/BiOI nanofibers: Facile fabrication with enhanced visible-light photocatalytic performance, *Mater. Res. Bull.* **111**, 202 (2019).
58. S. Begum and Md. Ahmaruzzaman, Biogenic synthesis of SnO2/activated carbon nanocomposite and its application as photocatalyst in the degradation of naproxen, *Appl. Surf. Sci.* **449**, 780 (2018).
59. U. O. Bhagwat, J. J. Wu, A. M. Asiri, and S. Anandan, Sonochemical Synthesis of Mg-TiO2 nanoparticles for persistent Congo red dye degradation, *J. Photochem. Photobiol. Chem.* **346**, 559 (2017).